High-Performance Lateral Metal-Germanium-Metal SWIR Photodetectors Using a-Si:H Interlayer for Dark Current Reduction

Harshvardhan Kumar 🅾, *Member, IEEE*, and Chu-Hsuan Lin 🅾, *Member, IEEE*

Abstract—In this work, we propose the lateral metal-germanium-metal photodetectors (PDs) structure on the silicon-on-insulator platform for short-wave infrared (SWIR) applications. The proposed device utilizes the highly *n*-doped amorphous silicon (a-Si:H) interlayer between metallic contact and low *n*-doped germanium active region to achieve a low dark current. Additionally, the tuning of Schottky barrier height (SBH) by the selection of various metallic contacts (Cr/W/Mo) has been investigated in order to achieve a large reduction in dark current. With a-Si:H interlayer and Mo metallic contacts at both anode and cathode terminals, the simulated energy band diagram shows that an effective increase in SBH of 0.17 eV and 0.766 eV for electrons and holes, respectively, and thus acts as barriers for electron and hole dark currents. The result shows that the Mo metallic contact device manifests the least dark current (dark current density) of 0.27 pA (0.027 mA/cm^2) at V_{bias} of 0.25 V and compared to Cr contact, it has been significantly decreased by two orders of magnitude. In addition, with Mo contact, the proposed device achieves the photogenerated-to-dark current (I_{ph}/I_{dark}) ratio and the responsivity of $\sim 1.7 \times 10^6$ and 0.96 A/W, respectively at $\lambda = 1.55$ μm with V_{bias} of 0.25 V. Furthermore, the proposed Mo-Ge-Mo PD shows high detectivity (NEP) of 9×10^{11} cmHz$^{1/2}$W^{-1} ($\sim 3 \times 10^{-16}$ WHz$^{-0.5}$), which is nearly 15 (one order lower) times higher than those of Cr-Ge-Cr PD. The results hold great potential for optoelectronic applications requiring low-power Ge-based PD.

Index Terms—High-performance, high detectivity, high sensitivity, low dark current, photodetectors, short-wave infrared.

I. INTRODUCTION

APPLICATION for light detection in the short-wave infrared (SWIR) regime (1–8 μm) ranges from fiber-optic telecommunications [1] to the detection of trace gases [2], biomedical [3], [4], [5], imaging, and night-time surveillance[6], etc. Currently, the optical components working in the low-loss window (1.3–1.6 μm) have completely replaced the earlier metal interconnects, due to their extremely high data exchange rate

(>10 GB/s) [7]. In the past decade, a variety of photodetectors (PDs) using Ge, InGaAs, PbS, and HgCdTe are being used in SWIR bands [8], [9], [10], [11]. Among these, lattice-matched InGaAs/InP detectors have proved to be the most efficient PD for SWIR (0.9–1.7 μm) applications because of their excellent quantum efficiency and low dark current at ambient temperature[12]. However, the present Si IC technology is incompatible with the III–V and II–VI compounds [13]. Ge, on the other hand, offers inherent benefits over the current III-V and II-VI compounds, including a high SWIR band absorption coefficient, low cost, and compatibility with CMOS technology [14], [15]. Therefore, Ge-based PDs can be a potential optical device for advanced group-IV photonics technology (more precisely known as Si photonics). Additionally, Ge metal-semiconductor-metal (MSM) PDs have a number of benefits over Ge *p-i-n* and avalanche PDs, including reduced junction capacitance, ease of fabrication, and high bandwidth[16], [17]. However, the thermionic emission at the Schottky contact and low electron and hole Schottky barrier height (SBH) result in a large dark current of MSM PDs. As a result, Ge MSM PDs result in poor detectivity and sensitivity. The high shot and thermal noise currents, which can also be caused by the large dark current, can lead to low signal-to-noise ratios (SNR) and excessive power consumption of PDs.

In recent years, to reduce the dark current of Ge MSM PDs, several techniques have been employed. For example, the insertion of a thin layer of wide bandgap materials between the metal contact and Ge such as SiC [18], a-Ge [19], and the introduction of TiO$_2$ as an interlayer [20]. In addition, the introduction of asymmetric metal contacts has also been employed to suppress the dark current [8]. Based on the literature, it can be concluded that the introduction of wide bandgap materials significantly affects the diminution of dark current [18]. However, the use of the above techniques may result in poor quantum efficiency due to the limited collection of photogenerated carriers. Recently, Dushaq et al. reported reduced dark current Ge-on-Si (GOS) MSM PD using a-Si:H interlayer without affecting the photogenerated carrier's collection [7]. However, still, Ge MSM PD's performance is not comparable with the commercially available Ge and InGaAs PDs [9], [21]. This makes it difficult to develop high-performance (in terms of high responsivity and low dark current) Ge MSM PDs for SWIR applications. Therefore, it is necessary to investigate the techniques to reduce the dark current by large orders to achieve high-performance PDs in terms of

Harshvardhan Kumar is with the Department of Electronics and Communication Engineering, The LNM Institute of Information Technology, Jaipur, RJ 302031, India (e-mail: harshvardhan.kumar@lnmiit.ac.in).

Chu-Hsuan Lin is with the Department of Optoelectronics, National Dong Hwa University, Hualien County 974, Taiwan (e-mail: chlin0109@gms.ndhu.edu.tw).

high on-off ratio, responsivity, detectivity, and sensitivity in the SWIR regime.

In this work, we study theoretically the lateral Ge MSM PDs on silicon-on-insulator (SOI) platform using finite element method (FEM) simulations. To minimize the dark current, the proposed PD structure utilizes a thin layer of amorphous silicon (a-Si:H) between the metal contact and the Ge active layer. Moreover, over the Si platform, the SOI substrate provides low junction capacitance, thus resulting in high speed 3dB bandwidth. Also, the SOI platform helps in reducing power consumption. In the proposed lateral structure, the metal contacts are placed far away resulting in low reflectivity of the incident light, and thus, high optical confinement can be found in Ge active layer. Here, we have also investigated the effect of different metallic contacts such as chromium (Cr), tungsten (W), and molybdenum (Mo) to get high electron and hole SBH, and thus a significant reduction in dark current can be obtained. The impact of the distance between two electrodes and the thickness of the Ge active layer on the frequency response of the proposed PD has also been studied. Finally, we have optimized the proposed device structure to achieve high responsivity, detectivity, and sensitivity at SWIR bands.

II. DEVICE DESIGN AND MODELING

The FEM simulation of the proposed two-dimensional (2-D) device structure has been done using COMSOL Multiphysics software using the electrostatic mode (to calculate the energy band diagram and dark current). In this mode, the governing continuity equation combined with Gauss's law is given as [22];

$$\nabla \cdot (-\epsilon_0 \epsilon_r \nabla V) = \rho \qquad (1)$$

where, ϵ_0 and ϵ_r are the free-space permittivity and relative permittivity of the material, respectively. V and ρ are the electrostatic potential and space-charge density, respectively. To study the impact of illumination on the proposed MSM PD, we have used semiconductor-electromagnetic wave coupling (multiphysics) and the governing equation for the electromagnetic wave (frequency domain, 2-D structure) can be given as [23];

$$\nabla \times \mu_r^{-1} (\nabla \times E) - k_0^2 \left(\epsilon_r - \frac{i\sigma}{\omega \epsilon_0} \right) E = 0 \qquad (2)$$

$$E(x, y, z) = \tilde{E}(x, y) \exp(-i k_z z) \qquad (3)$$

where, μ_r is the relative permeability and σ is the conductivity of the material. k_0 and k_z are the free-space and out-of-plane wave numbers, respectively. ω is the angular frequency and E is the electric field.

In this study, a plane wave is used as the light source (0.5 μW in the spectral range of 1.2–1.9 μm) normally incident on the proposed lateral Ge MSM structure, and FEM analysis is used to quantify the reflection loss (in terms of reflectivity). By using an anti-reflective coating, the reflection loss can be greatly decreased (discussed *in-depth* later). On the Ge PD surface at 1550 nm, the simulation reveals a low reflection loss (20%). As a result, the EQE may possibly be higher than 75% to enable sensitive photodetection. A 250-W quartz tungsten halogen (QTH) lamp can be used to measure the reflectivity
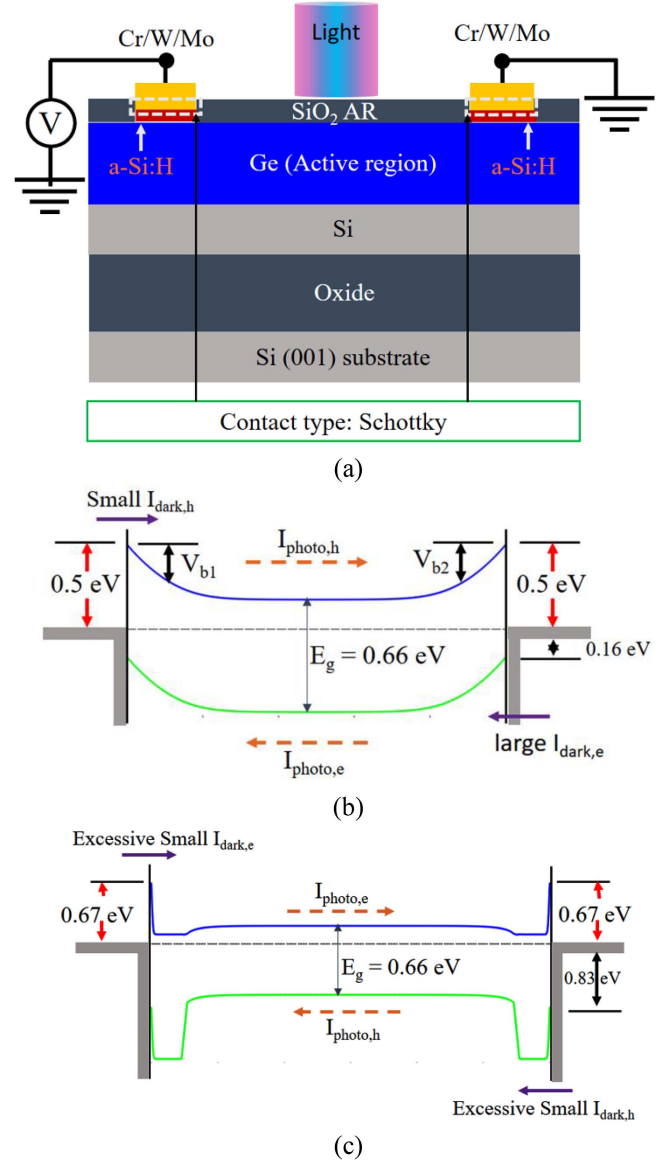

Fig. 1. (a) Two-dimensional schematic of our designed lateral Ge metal-semiconductor-metal photodetectors with a-Si:H interlayer. Simulated energy band diagram and flow of currents of the proposed device [device-C] (b) Without and (c) With a-Si:H interlayer.

(reflection loss) and optical responsivity for the real (fabricated) device. Using a microscope, the light source will be scattered by a monochromator, chopped at 190 Hz, and then incident normally on the Ge MSM PDs [24]. A commercially available extended InGaAs PD (S148C, Thorlabs) can detect the reflected light intensity to determine the reflectivity (reflection loss) [24].

The 2-D schematic of the proposed device structure on the SOI platform with a cross-sectional area of 30 μm^2 is depicted in Fig. 1(a). Both electrodes (anode and cathode terminals) are of Schottky contact (metal-semiconductor) with a thin a-Si:H interlayer. To achieve the highest photodetection efficiency, it is required to deplete the Ge active region. Therefore, particularly, the a-Si:H interlayer is kept highly doped and the Ge active layer is lightly doped to keep the maximum depletion region in the

TABLE I
VALUES OF BANDGAP ENERGY AND ELECTRON AFFINITY OF GE AND A-SI:H
INTERLAYER [25], [26], [27]

Material	Bandgap (eV)	Electron affinity (eV)
Ge	0.664	4.0
a-Si:H	1.5	3.93

TABLE II
THE VALUES OF WORK FUNCTION METAL USED IN THIS WORK [28]

Metals	Work function φ_M (eV)
Chromium (Cr)	4.5
Tungsten (W)	4.55
Molybdenum (Mo)	4.6

TABLE III
CALCULATED VALUES OF ELECTRON AND HOLE SBH WITHOUT AND WITH
A-SI:H INTERLAYER

Device(s)	MSM	SBH (in eV)			
		Without a-Si:H		With a-Si:H	
		φ_e	φ_p	φ_e	φ_p
A	Cr-Ge-Cr	0.5	0.164	0.57	0.93
B	W-Ge-W	0.55	0.114	0.62	0.88
C	Mo-Ge-Mo	0.6	0.064	0.67	0.83

*Here, φ_e and φ_p are the electron and hole SBH, respectively.

Ge active region. The a-Si:H interlayer was highly n-type doped ($\sim 10^{19}$ cm^{-3}) and the 1-μm thick Ge active layer was lightly n-type doped ($\sim 10^{16}$ cm^{-3}). The bandgap energies electron affinities of the Ge and a-Si:H used in the simulation have been taken from [25], [26], [27] and their exact values are given in Table I. Three metal contacts (Cr/W/Mo) are considered in this work and their work function values are given in Table II.

The Mo-Ge-Mo PD's simulated energy band diagram without an a-Si:H interlayer is shown in Fig. 1(b). Additionally, it demonstrates the device's current flow mechanism. As shown in Fig. 1(b), electron SBH of $\sim$0.6 eV and a very low hole SBH of 0.064 eV form at the metal-semiconductor interfaces owing to severe Fermi-level pinning [7], [28], [29]. The device, therefore, shows a significant dark current.

Fig. 1(c) shows the energy band diagram of the proposed structure with the enhanced SBH for both electrons (0.67 eV) and holes (0.83 eV) by introducing a-Si:H interlayer between metal and Ge active layer. The large bandgap energy of a-Si:H ($\sim$1.5 eV) and high tunneling resistance can considerably suppress the dark current into the device without affecting the photogenerated carrier's collection.

In this work, we have considered three different devices such as device-A: Cr-Ge-Cr, device-B: W-Ge-W, and device-C: Mo-Ge-Mo. We estimated the SBH for all three devices (their values are given in Table III), both with and without an a-Si:H interlayer, to better understand the mechanism of dark current flow. The calculated values reveal that with the introduction of a-Si:H interlayer and by selecting the proper metal contact, electron and hole SBH can be enhanced by a large amount, and thus, significant dark current magnitude reduction of the device can
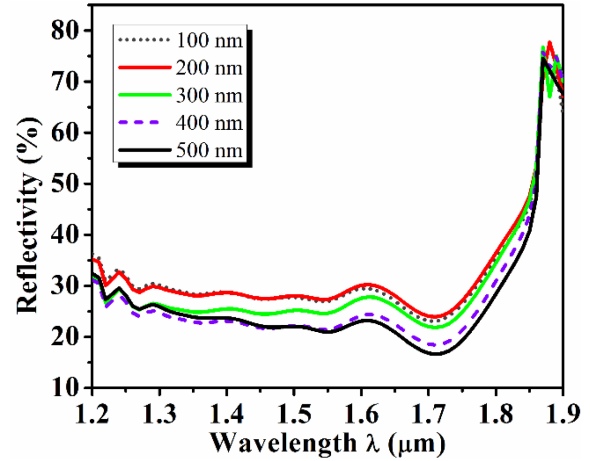

Fig. 2. The proposed device's simulated reflectivity spectra for various SiO$_2$ AR layer thicknesses.

be achieved. Based on the calculated values of SBH with a-Si:H interlayer, Device-C could perform the best among the other two devices in terms of decreased dark current, responsivity, detectivity, and sensitivity.

In addition, to get the minimum reflectivity of the incident light (reflection loss), the proposed PD structure is coated with the SiO$_2$ antireflective layer (AR). The low reflectivity of the normally incident light results in the high responsivity of the device. Fig. 2 shows the simulated reflectivity spectra of the device with different thicknesses of the SiO$_2$ layer. The result demonstrates that reflectivity slightly decreases with the increase of SiO$_2$ layer thickness and its values are nearly constant in the spectral region of 1.3–1.7 μm. For SiO$_2$ layer thickness of 100–500 nm, the reflectivity of the device lies between 20–30% in the spectral region of 1.3–1.7 μm. Therefore, in this work, from the fabrication perspective, the optimal SiO$_2$ layer thickness of 300 nm has been considered to calculate the device responsivity and other important metrics.

III. RESULTS AND DISCUSSION

A. Current-Voltage Characteristics

Usually, the current of the MSM devices increases exponentially with the applied voltage and may be fitted by the diode current equation (1), which suggests a thermionic emission at the metal-semiconductor heterointerface [28], [30]:

$$I(V) = J(V) * A = A * J_0 \left[\exp\left(\frac{qV}{\eta k_B T}\right) - 1 \right] \quad (4)$$

where A denotres the device cross-sectional area, q denotes the charge of an electron, V denotes the applied bias voltage, η denotes the ideality factor, k_B denotes the Boltzmann constant, and T denotes the absolute temperature (in K). J_0 denotes the saturation current density and the following equation may be used used to compute it [7], [28];
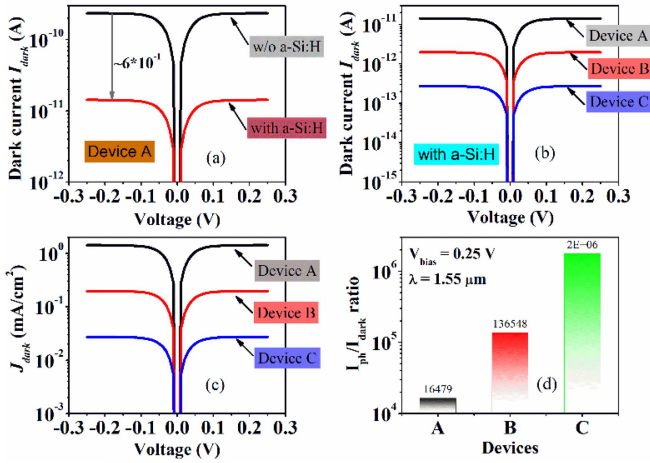
$$J_0 = A^* T^2 e^{-q\varphi_B/kT} \quad (5)$$

Fig. 3. (a) Variation of simulated dark current with the applied bias voltage for device-a without and with a-Si:H interlayer. (b) and (c) Dark current and dark current density for all proposed PDs with a-Si:H interlayer at ambient temperature. (d) Photogenerated-to-dark current ratio of all proposed PDs with a-Si:H interlayer at $\lambda = 1.55~\mu m$ for a fixed bias voltage of 0.25 V.

where A^* denotes the effective Richardson constant and φ_B denotes the SBH. By extrapolating as a y-axis intercept from the linear fluctuation of log(J) in forward bias, (4) may be utilised to determine the SBH between Ge/metal interface.

At room temperature, the simulated current-voltage (*I-V*), current density-voltage (*J-V*), and photogenerated-to-dark currents (I_{ph}/I_{dark}) ratio are all shown in Fig. 3. Fig. 3(a) demonstrates the dark current without and with a-Si:H interlayer for device-A. At V = 0.25 V, device-A designed without and with an interlayer exhibits a dark current of $\sim$0.23 nA and $\sim$14.2 pA, respectively. This result clearly indicates that the introduction of a-Si:H interlayer reduces the dark current of Device-A by nearly two orders. The large dark current of the proposed conventional device (without interlayer) is due to the severe Fermi-level pinning. Next, dark current (dark current density) for all three devices with an interlayer have also been estimated, as shown in Fig. 3(b) and (c). At V = 0.25 V, the dark current (dark current density) values are $\sim$14.2 pA ($\sim$1.42 mA/cm^2), $\sim$1.97 pA ($\sim$0.19 mA/cm^2), and $\sim$0.27 pA ($\sim$0.03 mA/cm^2) for device-A, B, and C, respectively. Based on these findings, it can be shown that device C has much lower dark current values than devices A and B. The behavior can be explained based on the increased electron and hole SBH for device-C. When comparing the findings of our work to those from other publications, the proposed work indicates a dark current for device-C of 0.27 pA, which is much less than the dark currents for previously reported devices of$\sim$1 μA [20] and $\sim$0.1 nA [7] (here, the comparison has been made at V = $\sim$0.25 V).

Fig. 3(d) shows the calculated photogenerated-to-dark current ratio for all three devices with an interlayer. All proposed devices show a very high value of I_{ph}/I_{dark} ratio due to high photogenerated carrier collection efficiency. However, particularly, device-C exhibits I_{ph}/I_{dark} ratio 107.1 and 12.93 times higher than those for device-A and B, respectively. This high value of I_{ph}/I_{dark} ratio for device-C is due to a very low dark current.
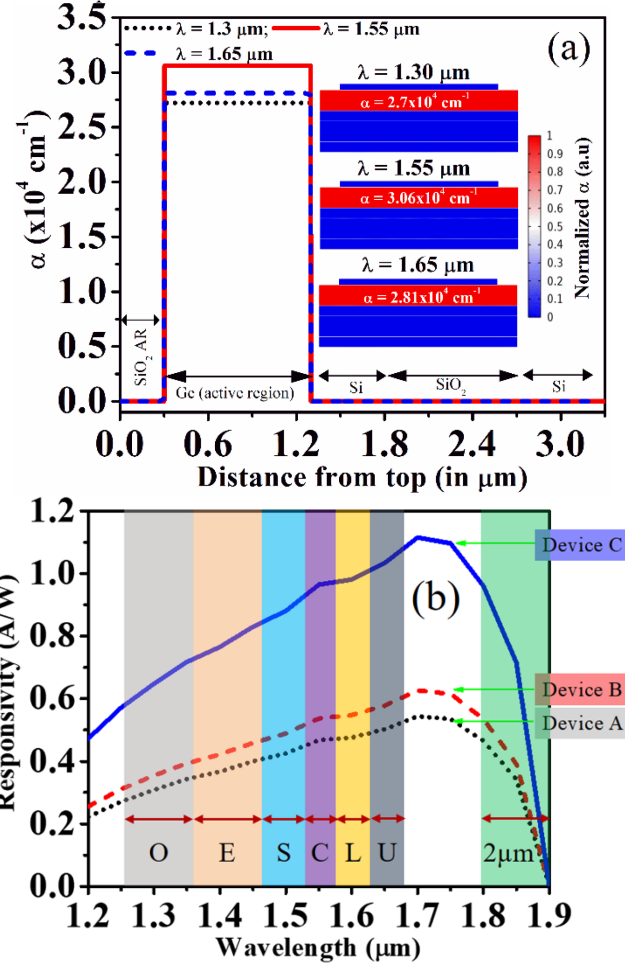

Fig. 4. (a) Simulated absorption coefficient of the proposed structure at room temperature. (b) Optical responsivity of the proposed PDs with a-Si:H interlayer at V = 0.25V.

B. Absorption Coefficient and Responsivity Spectra

The optical characteristics of the proposed PD have been investigated by calculating the absorption coefficient and optical responsivity in the 1.2–1.9 μm wavelength region. Fig. 4(a) shows the simulated absorption coefficient of various layers of the designed device at $\lambda = 1.3~\mu m$, 1.55 μm, and 1.65 μm. Typically, the absorption coefficient (α) is given as $\alpha \propto \sqrt{h\upsilon - E_g}$ and is greatly affected by the photon energy ($h\upsilon$) and material bandgap energy (E_g) [31]. The result shows that the absorption coefficient is zero for SiO$_2$ AR and SOI substrate. The large bandgap energy of Si (E$_g$ (Si) = 1.1 eV, which corresponds to an absorption cut-off wavelength of 1.1 μm), thus, makes Si-based PDs unsuitable for photodetection in the SWIR region. However, the Ge active layer offers a very high absorption coefficient at $\lambda = 1.3~\mu m$, 1.55 μm, and 1.65 μm. Therefore, the Ge active layer in this study is primarily responsible for the device's optical responsivity. The inset of Fig. 4(a) shows the normalized absorption coefficient of the Ge MSM PD at different operating wavelengths and its values for the Ge active layer are $\sim$2.7 $\times$ 10^4 cm^{-1}, $\sim$3.06 $\times$ 10^4 cm^{-1}, and $\sim$2.81 $\times$ 10^4 cm^{-1} at $\lambda = 1.3~\mu m$, 1.55 μm, and 1.65 μm, respectively. This

optical characteristic makes Ge-based PDs suitable for SWIR bands. The high absorption coefficient of Ge is mainly due to its quasi-direct bandgap nature and small bandgap energy.

The photoresponse of the Ge MSM PDs with an interlayer was then described for V = 0.25 V at room temperature in terms of optical responsivity. The optical responsivity ($\Re$) can be calculated using the relation, $\Re = I_{ph}/P_{in} = (I_{tot} - I_{dark})/P_{in}$ [32], where I_{ph} and P_{in} are the photogenerated current and the power of incident optical signal, respectively. For the proposed device with an a-Si:H interlayer, Fig. 4(b) illustrates the calculated responsivity with operating wavelength. The calculated responsivity spectra show that the proposed PDs can detect the optical signal in the SWIR range (1.2–1.7 μm). At = 1.55 m, Device-C has an optical responsivity of 0.96 A/W compared to Devices-A and B's respective values of 0.47 A/W and 0.54 A/W. The lower optical responsivity values of device-A and B are expected because of their high dark current. The above value for responsivity for device-C is higher compared to earlier reported results of Ge MSM PD with calculated responsivity in the range of 0.1–0.6 A/W at $\lambda = 1.55$ μm [7], [33]. The suggested device's high responsivity is a result of its low optical losses and reduced dark current.

C. Analysis of Detectivity and NEP

Another important optoelectronic metrics of the PD are detectivity (D^*) and the noise-equivalent-power (NEP). The detectivity explains the smallest optical signal (minimum detectable power) that can be detected in the midst of noise. On the contrary, NEP measures the PD's sensitivity and by taking the inverse of NEP, one may calculate the device's sensitivity. Therefore, high detectivity and low NEP are desired for high-performance PDs. Mathematically, the detectivity and NEP, can be calculated as [27], [32], [34], [35], [36];

$$D^* = \frac{\Re(A)^{1/2}}{(2qI_{dark})^{1/2}} \tag{6}$$

$$NEP = \frac{i_n}{\Re} = \frac{\sqrt{2qI_{dark}\Delta f}}{\Re} \tag{7}$$

where $\Re$ denotes the optical responsivity, A denotes the illumination area (in cm^2), q denotes the charge of an electron, I_{dark} denotes the dark current, and Δf denotes the bandwidth (here, $\Delta f = 1$ Hz has been considered [34]). Equations (6)-(7) reveal that the reduced dark current for the PDs will lead to high detectivity and sensitivity. The calculated detectivity and NEP values under V = 0.25 V for all devices are shown in Fig. 5(a) and (c), respectively, and their comparative values at $\lambda = 1.55$ μm for all devices are shown in Fig. 5(b) and (d), respectively. At $\lambda = 1.55$ μm, the peak values of detectivity are 6×10^{10}, 2×10^{11}, and 9×10^{11} cmHz$^{1/2}$W^{-1} for device-A, B, and C, respectively. Similarly, at $\lambda = 1.55$ μm, the minimum values of NEP are $\sim 5 \times 10^{-15}$, $\sim 1 \times 10^{-15}$, and $\sim 3 \times 10^{-16}$ W/Hz$^{0.5}$ for device-A, B, and C, respectively. Based on these calculated results, it can be concluded that device-C is better than A and B under V = 0.25 V at $\lambda = 1.55$ μm. Device-C exhibits high detectivity and low NEP due to its significant reduction of dark current and high optical responsivity. Additionally, all three
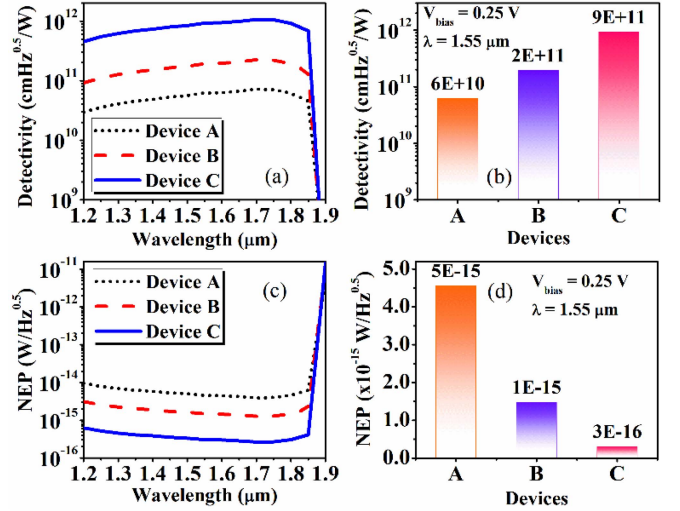

Fig. 5. Calculated detectivity and NEP of the proposed Ge MSM PD with a-Si:H interlayer. (a) and (c) Detectivity and NEP as a function of wavelength, respectively. (b) and (d) Detectivity and NEP values for device-A, B, and C at $\lambda = 1.55$ μm for a fixed bias voltage of 0.25 V.

proposed devices (A, B, and C) have detectivity values that are equivalent to or even greater than the currently available Ge PDs at $\lambda = 1.55$ μm [21], [37].

D. Frequency Response: 3dB Bandwidth

In photonic integrated circuit (PIC) systems, PD is one of the important optical devices, used to detect the modulated optical signal at high speed. Thus, the key metric of PD is 3dB bandwidth (f_{3dB}). Generally, the 3dB bandwidth of PD depends on both the RC time constant and carriers' transit time (time taken by the photogenerated carriers to travel through the Ge active region before being collected by the contacts). To reduce the RC time constant, the junction capacitance (C_{pd}) and load resistance (R_L) should be small. Furthermore, the transit time of MSM PD can be reduced by minimizing the distance between two electrodes. The RC-limited, transit time-limited, and overall 3dB bandwidths of the PD can be calculated using [27], [32], [33], [34];

$$f_{RC} = \frac{1}{2\pi R_L C_{pd}} \tag{8}$$

$$f_t = \frac{3.5v}{2\pi d_{abs}} \tag{9}$$

$$f_{3dB} = \left[\left(\frac{1}{f_{RC}}\right)^2 + \left(\frac{1}{f_t}\right)^2\right]^{-1/2} \tag{10}$$

where v is the drift velocity of Ge ($\sim 6.5 \times 10^6$ cm/s [38]) and d_{abs} denotes the seperation between two electrodes. The junction capacitance for the proposed PD is 1.13 fF and the load resistance of 50 Ω, has been considered to calculate the bandwidth of the designed device (Fig. 6).

As shown in Fig. 6(a) shows the calculated RC and transit time-limited bandwidths as a function of the distance between
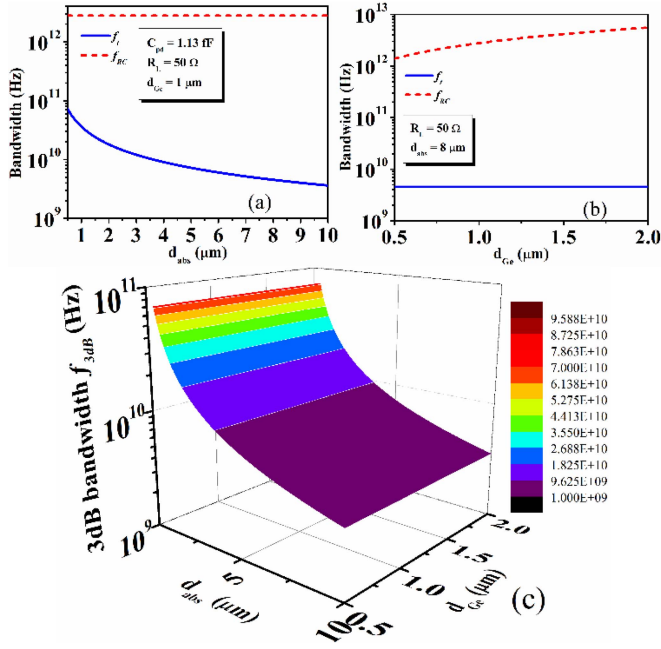
Fig. 6. Calculated RC and transit time-limited bandwidth as a function of (a) Distance between two electrodes and (b) Ge active layer thickness. (c) Variation of 3dB cut-off frequency with the distance between two electrodes and Ge active layer thickness.

TABLE IV
CALCULATED RBW PRODUCT FOR THE PROPOSED PD AT ROOM TEMPERATURE

Proposed PD	Devices		
	A	B	C
RBW product (A-GHz/W)	33.84	38.88	69.12

two electrodes. We can observe that f_{RC} is independent of d_{abs} but f_t of PD strongly depends on d_{abs}. f_t decreases with the increasing d_{abs}. Comparatively, Fig. 6(b) demonstrates the calculated RC and transit time-limited bandwidths with the varying Ge active layer thickness (d_{Ge}). The result reveals that the Ge active thickness doesn't have any impact on f_t, however, f_{RC} increases with the increasing d_{Ge}. Fig. 6(c) demonstrates the calculated 3dB cut-off frequency as a function of d_{abs} and d_{Ge}. f_{3dB} decreases significantly with the increase of d_{abs}, however, it is nearly constant with the increase of d_{Ge}. In other words, f_{3dB} is strongly affected by the distance between electrodes and it is less affected or unaffected by the change in active layer thickness. Therefore, it can be concluded that f_{3dB} is mainly limited by the carriers' transit time for the proposed MSM PD. Thus, if the distance between two electrodes is small, then high 3dB bandwidth can be achieved. Next, the responsivity-bandwidth (RBW) product can be estimated using (10) and expression for responsivity (given in Section III-B). Their calculated values for all proposed devices are given in Table IV. Generally, high RBW product is desired for high-performance PD in order to achieve high-speed and photosensitivity. The active layer thickness, however, causes a *trade-off* between the optical responsivity and bandwidth. In this work, this *trade-off* has been

TABLE V
PROPOSED PD'S ESTIMATED ENERGY CONSUMPTION VALUES AT ROOM TEMPERATURE

Proposed PD	Devices		
	A	B	C
E_p	0.24 fJ/bit	0.21 fJ/bit	0.12 fJ/bit

TABLE VI
COMPARATIVE ANALYSIS OF PERFORMANCES OF EARLIER REPORTED GE MSM PDS AT ROOM TEMPERATURE

Ge PDs	J_{dark} (A/cm²)	I_{dark}	$\Re$ (A/W)	λ (μm)	S/E*
Ge-on-SOI[18]	8.52×10^{-2}	11.5 nA @1V	0.53	1.55	E
Ge-on-Si[41]	0.025	100 nA @-1V	0.12	1.55	E
Ge-on-Si[8]	0.1	--	0.85	1.55	E
Ge bulk[20]	2.8×10^{-2}	2.8 μA @1V	0.18	1.55	E
Ge-on-Si[42]	$\sim 1 \times 10^{-5}$	---	~ 0.6	1.55	S
Ge[32]	9×10^{-6}	0.54 pA@-2V	~ 0.82	1.55	S
Ge[43]	----	10 nA @1.6V	---	---	S
This work (Ge-on-SOI)	3×10^{-5}	0.27 pA @0.25V	0.96	1.55	-

*S: Simulation; E: Experimental

reduced by optimizing the active Ge layer thickness and the distance between electrodes. Thus, the proposed device exhibits high value of responsivity and bandwidth as well. As a result, RBW product is significantly higher for our designed device. Considering the distance between electrodes of 0.5 μm and Ge layer thickness of 1 μm, the f_{RC}, f_t, and f_{3dB} of the proposed PDs are ~2.8 THz, ~72.4 GHz, and ~72 GHz, respectively. These high bandwidths show the potential for the realization of high-speed PDs for SWIR applications.

E. Energy Consumption of Proposed PD

Estimating the received optical energy (E_p) desired for a bit allows for the analysis of PD's energy consumption and it can be expressed as [39], [40];

$$E_p = C_{pd}V_d hc/\lambda \eta q \tag{11}$$

where, C_{pd} denotes the PD's junction capacitance and h is the Planck's constant. V_d denotes the front-end amplifier's signalling voltage (in this work, $V_d = 100$ mV has been taken into consideration [40]). c denotes the speed of the free-space light, λ denotes the PD's operating wavelength, and q denotes the charge of an electron. η denotes the PD's external quantum efficiency ($\eta \leq 1$) and it can be calculated as, $\eta = 1240\Re/\lambda$ [32], where, $\Re$ denotes the spectral responsivity. The computed values of energy consumption of PDs expressed in terms of energy/bit (E_p) (E p) for all devices are given in Table V.

The overview and comparison of several metrics of previously published Ge PDs are shown in Table VI. This study demonstrates that by introducing an a-Si:H interlayer between the metal and the Ge active layer and by selecting the Mo metal contact for both electrodes, it is possible to obtain reduced dark current, excellent detectivity, sensitivity, and responsivity. In addition,

lateral structure on the SOI platform has great potential for high-performance PDs in PICs for SWIR applications.

IV. Conclusion

In conclusion, we have proposed the lateral metal-germanium-metal PDs using a-Si:H interlayer for the dark current reduction. The effect of various metallic contacts on the dark current of the PDs has also been investigated. Mo metallic contact at both the anode and cathode terminals reduced the dark current of the Ge MSM PD by one and two orders, as compared with W-Ge-W and Cr-Ge-Cr MSM PDs, respectively, due to its enhanced SBH. Moreover, the proposed PD with Mo contacts also showed record high responsivity (>0.96 A/W), detectivity (9×10^{11} cmHz$^{1/2}$W^{-1}), and sensitivity (2.5×10^5 cm^2/W) for V_{bias} of 0.25V at $\lambda = 1.55$ μm. These values are higher compared with Cr-Ge-Cr and W-Ge-W MSM PDs. The frequency response of the device showed that 3dB bandwidth depends significantly on the distance between both electrodes (it is significantly affected by the carriers' transit time), however, it is less dependent on the Ge active layer thickness. The proposed PD with high responsivity, detectivity, sensitivity, and large photogenerated-to-dark current ratio enables it for future low-power and high-performance optoelectronic applications.

References

[1] W. Hu et al., "Germanium/perovskite heterostructure for high-performance and broadband photodetector from visible to infrared telecommunication band," *Light Sci. Appl.*, vol. 8, no. 1, pp. 1–10, 2019, doi: 10.1038/s41377-019-0218-y.

[2] N. Amoosoltani, A. Zarifkar, and A. Farmani, "Particle swarm optimization and finite-difference time-domain (PSO/FDTD) algorithms for a surface plasmon resonance-based gas sensor," *J. Comput. Electron.*, vol. 18, no. 4, pp. 1354–1364, 2019, doi: 10.1007/s10825-019-01391-7.

[3] H. Xu, J. Liu, J. Zhang, G. Zhou, N. Luo, and N. Zhao, "Flexible organic/inorganic hybrid near-infrared photoplethysmogram sensor for cardiovascular monitoring," *Adv. Mater.*, vol. 29, no. 31, 2017, Art. no. 1700975, doi: 10.1002/adma.201700975.

[4] M. A. Baqir, A. Farmani, T. Fatima, M. R. Raza, S. F. Shaukat, and A. Mir, "Nanoscale, tunable, and highly sensitive biosensor utilizing hyperbolic metamaterials in the near-infrared range," *Appl. Opt.*, vol. 57, no. 31, pp. 9447–9454, 2018, doi: 10.1364/AO.57.009447.

[5] S. Park et al., "Ultraflexible near-infrared organic photodetectors for conformal photoplethysmogram sensors," *Adv. Mater.*, vol. 30, no. 34, 2018, Art. no. 1802359, doi: 10.1002/adma.201802359.

[6] E. H. Sargent, "Solar cells, photodetectors, and optical sources from infrared colloidal quantum dots," *Adv. Mater.*, vol. 20, no. 20, pp. 3958–3964, 2008, doi: 10.1002/adma.200801153.

[7] G. Dushaq, A. Nayfeh, and M. Rasras, "Metal-germanium-metal photodetector grown on silicon using low temperature RF-PECVD," *Opt. Exp.*, vol. 25, no. 25, pp. 32110–32119, 2017, doi: 10.1364/oe.25.032110.

[8] A. K. Okyay, A. M. Nayfeh, K. C. Saraswat, T. Yonehara, A. Marshall, and P. C. McIntyre, "High-efficiency metal-semiconductor-metal photodetectors on heteroepitaxially grown Ge on Si," *Opt. Lett.*, vol. 31, no. 17, pp. 2565–2567, 2006, doi: 10.1364/ol.31.002565.

[9] M. J. Cohen, M. H. Ettenberg, M. J. Lange, and G. H. Olsen, "Commercial and industrial applications of indium gallium arsenide near-infrared focal plane arrays," *Proc. SPIE*, vol. 3698, pp. 453–461, 1999, doi: 10.1117/12.354547.

[10] J. He et al., "Synergetic effect of silver nanocrystals applied in PbS colloidal quantum dots for high-performance infrared photodetectors," *ACS Photon.*, vol. 1, no. 10, pp. 936–943, 2014, doi: 10.1021/ph500227u.

[11] A. Rogalski, J. Antoszewski, and L. Faraone, "Third-generation infrared photodetector arrays," *J. Appl. Phys.*, vol. 105, no. 9, 2009, Art. no. 091101, doi: 10.1063/1.3099572.

[12] M. P. Hansen and D. S. Malchow, "Overview of SWIR detectors, cameras, and applications," *Thermosense XXX*, vol. 6939, 2008, Art. no. 69390I, doi: 10.1117/12.777776.

[13] J. Wang and S. Lee, "Ge-photodetectors for Si-based optoelectronic integration," *Sensors*, vol. 11, no. 1, pp. 696–718, 2011, doi: 10.3390/s110100696.

[14] J. Michel, J. Liu, and L. C. Kimerling, "High-performance Ge-on-Si photodetectors," *Nature Photon.*, vol. 4, no. 8, pp. 527–534, 2010, doi: 10.1038/nphoton.2010.157.

[15] D. Feng et al., "High-speed Ge photodetector monolithically integrated with large cross-section silicon-on-insulator waveguide," *Appl. Phys. Lett.*, vol. 95, no. 26, 2009, Art. no. 261105, doi: 10.1063/1.3279129.

[16] L. Vivien et al., "High speed and high responsivity germanium photodetector integrated in a silicon-on-insulator microwaveguide," *Opt. Exp.*, vol. 15, no. 15, 2007, Art. no. 9843, doi: 10.1364/oe.15.009843.

[17] L. Chen and M. Lipson, "Ultra-low capacitance and high speed germanium photodetectors on silicon," *Opt. Exp.*, vol. 17, no. 10, 2009, Art. no. 7901, doi: 10.1364/oe.17.007901.

[18] K. W. Ang et al., "Novel silicon-carbon (Si:C) Schottky barrier enhancement layer for dark-current suppression in Ge-on-SOI MSM photodetectors," *IEEE Electron Device Lett.*, vol. 29, no. 7, pp. 704–707, Jul. 2008, doi: 10.1109/LED.2008.923540.

[19] J. Oh, S. K. Banerjee, and J. C. Campbell, "Metal-germanium-metal photodetectors on heteroepitaxial Ge-on-Si with amorphous Ge Schottky barrier enhancement layers," *IEEE Photon. Technol. Lett.*, vol. 16, no. 2, pp. 581–583, Feb. 2004, doi: 10.1109/LPT.2003.822258.

[20] H.-J. Zang, G.-S. Kim, G.-J. Park, Y.-S. Choi, and H.-Y. Yu, "Asymmetrically contacted germanium photodiode using a metal–interlayer–semiconductor–metal structure for extremely large dark current suppression," *Opt. Lett.*, vol. 41, no. 16, pp. 3686–3689, 2016, doi: 10.1364/ol.41.003686.

[21] J. W. Zeller et al., "Development of Ge PIN photodetectors on 300 mm Si wafers for near-infrared sensing," *Int. J. Eng. Res. Technol.*, vol. 8, no. 1, pp. 23–33, 2015.

[22] COMSOL Multiphysics, "Semiconductor module," 2018. [Online]. Available: https://doc.comsol.com/5.6/doc/com.comsol.help.semicond/SemiconductorModuleUsersGuide.pdf

[23] "Wave optics module," 2018. [Online]. Available: https://doc.comsol.com/5.4/doc/com.comsol.help.woptics/WaveOpticsModuleUsersGuide.pdf

[24] B.-J. Huang, J.-H. Lin, H. H. Cheng, and G.-E. Chang, "GeSn resonant-cavity-enhanced photodetectors on silicon-on-insulator platforms," *Opt. Lett.*, vol. 43, no. 6, pp. 1215–1218, 2018, doi: 10.1364/OL.43.001215.

[25] G. Dushaq, A. Nayfeh, and M. Rasras, "Tuning the optical properties of RF-PECVD grown μc-Si:H thin films using different hydrogen flow rate," *Superlattices Microstructures*, vol. 107, pp. 172–177, 2017, doi: 10.1016/j.spmi.2017.03.052.

[26] R. Biron, C. Pahud, F. J. Haug, J. Escarré, K. Söderström, and C. Ballif, "Window layer with p doped silicon oxide for high V oc thin-film silicon nip solar cells," *J. Appl. Phys.*, vol. 110, no. 12, 2011, Art. no. 124511, doi: 10.1063/1.3669389.

[27] H. Kumar and R. Basu, "Design of mid-infrared Ge1-x Sn x homojunction pin photodiodes on Si substrate," *IEEE Sens. J.*, vol. 22, no. 8, pp. 7743–7751, Apr. 2022, doi: 10.1109/JSEN.2022.3159833.

[28] D. A. Neamen, *Semiconductor Physics and Devices*. 4th ed. New York: McGraw-Hill, 2021.

[29] A. Dimoulas, P. Tsipas, A. Sotiropoulos, and E. K. Evangelou, "Fermi-level pinning and charge neutrality level in germanium," *Appl. Phys. Lett.*, vol. 89, no. 25, pp. 12–15, 2006, doi: 10.1063/1.2410241.

[30] R. Hussin, Y. Chen, and Y. Luo, "Metal-semiconductor-metal heterojunction diodes consisting of a thin layer of crystal silicon," *Appl. Phys. Lett.*, vol. 102, no. 9, 2013, Art. no. 093507, doi: 10.1063/1.4794421.

[31] M. Kurosawa, M. Kato, T. Yamaha, N. Taoka, O. Nakatsuka, and S. Zaima, "Near-infrared light absorption by polycrystalline SiSn alloys grown on insulating layers," *Appl. Phys. Lett.*, vol. 106, no. 17, 2015, Art. no. 171908, doi: 10.1063/1.4919451.

[32] H. Kumar, A. K. Pandey, and C.-H. Lin, "Optimal design and noise analysis of Germanium (Ge) photodetectors for SWIR applications," *IEEE J. Electron. Devices Soc.*, vol. 10, pp. 649–659, 2022, doi: 10.1109/JEDS.2022.3195210.

[33] J. Gosciniak and M. Rasras, "High-bandwidth and high-responsivity waveguide-integrated plasmonic germanium photodetector," *J. Opt. Soc. Amer. B*, vol. 36, no. 9, pp. 2481–2491, 2019, doi: https://doi.org/10.1364/JOSAB.36.002481.

[34] H. Kumar and A. K. Pandey, "GeSn-Based multiple-quantum-well photodetectors for mid-infrared sensing applications," *IEEE Trans. Nanobiosci.*, vol. 21, no. 2, pp. 175–183, Apr. 2022, doi: 10.1109/TNB.2021.3136571.

[35] G. A. Saenz, G. Karapetrov, J. Curtis, and A. B. Kaul, "Ultrahigh photoresponsivity in suspended metal-semiconductor-metal mesoscopic multilayer MoS2 broadband detector from UV-to-IR with low schottky barrier contacts," *Sci. Rep.*, vol. 8, no. 1, pp. 1–11, 2018, doi: 10.1038/s41598-018-19367-1.

[36] A. Pradhan, S. Mukherjee, T. Maitra, A. Nayak, and S. Bhunia, "Improved spectral and temporal response of MSM photodetectors fabricated on MOCVD grown spontaneous AlGaAs superlattice," *Sensors Actuators, A Phys.*, vol. 297, 2019, Art. no. 111548, doi: 10.1016/j.sna.2019.111548.

[37] Y. Lin, K. H. Lee, B. Son, and C. S. Tan, "Low-power and high-detectivity Ge photodiodes by in-situ heavy As doping during Ge-on-Si seed layer growth," *Opt. Exp.*, vol. 29, no. 3, pp. 2940–2952, 2021, doi: 10.1364/oe.405364.

[38] Y. Zhang et al., "A high-responsivity photodetector absent metal-germanium direct contact," *Opt. Exp.*, vol. 22, no. 9, pp. 11367–11375, 2014, doi: 10.1364/oe.22.011367.

[39] P. Wahl et al., "Energy-per-bit limits in plasmonic integrated photodetectors," *IEEE J. Sel. Topics Quantum Electron.*, vol. 19, no. 2, Mar./Apr. 2013, Art. no. 3800210, doi: 10.1109/JSTQE.2012.2227687.

[40] D. A. B. Miller, "Device requirements for optical interconnects to silicon chips," *Proc. IEEE*, vol. 97, no. 7, pp. 1166–1185, Jul. 2009, doi: 10.1109/JPROC.2009.2014298.

[41] H. Zang et al., "Dark-current suppression in metal-germanium-metal photodetectors through dopant-segregation in NiGe–Schottky barrier," *IEEE Electron. Device Lett.,* vol. 29, no. 2, pp. 161–164, Feb. 2008, doi: 10.1109/LED.2007.914095.

[42] A. De Iacovo, A. Ballabio, J. Frigerio, L. Colace, and G. Isella, "Design and simulation of Ge-on-Si photodetectors with electrically tunable spectral response," *J. Light. Technol.*, vol. 37, no. 14, pp. 3517–3525, 2019, doi: 10.1109/JLT.2019.2917590.

[43] B. Arunachalam, Q. Rafhay, D. Roy, and A. Kaminski-Cachopo, "Simulation study of high-speed Ge photodetector dark and light current degradation," *IEEE Trans. Device Mater. Rel.*, vol. 22, no. 3, pp. 410–416, Sep. 2022, doi: 10.1109/TDMR.2022.3185671.